ELSEVIER

Cell Calcium 38 (2005) 141–152

cell calcium

www.elsevier.com/locate/ceca

Amplitude modulation of nuclear Ca^{2+} signals in human skeletal myotubes: A possible role for nuclear Ca^{2+} buffering

Werner J.H. Koopman [a,b], Peter H.G.M. Willems [a,b,*], Arie Oosterhof [a], Toin H. van Kuppevelt [a], Stan C.A.M. Gielen [c]

[a] *Department of 160 Biochemistry NCMLS, Radboud University Nijmegen Medical Center, P.O. Box 9101, Geert Grooteplein 28-30, NL-6500 HB, Nijmegen, The Netherlands*

[b] *Microscopical Imaging Center, NCMLS, Radboud University Nijmegen Medical Center, Geert Grooteplein 28-30, 6500 HB, Nijmegen, The Netherlands*

[c] *Department of Medical Physics and Biophysics, Radboud University Nijmegen, Geert Grooteplein 21, CPK1 231, 6525 EZ, Nijmegen, The Netherlands*

Received 21 December 2004; received in revised form 17 May 2005; accepted 2 June 2005
Available online 28 July 2005

Abstract

Video-rate confocal microscopy of Indo-1-loaded human skeletal myotubes was used to assess the relationship between the changes in sarcoplasmic ($[Ca^{2+}]_S$) and nuclear ($[Ca^{2+}]_N$) Ca^{2+} concentration during low- and high-frequency electrostimulation. A single stimulus of 10 ms duration transiently increased $[Ca^{2+}]$ in both compartments with the same time of onset. Rate and amplitude of the $[Ca^{2+}]$ rise were significantly lower in the nucleus (4.0- and 2.5-fold, respectively). Similarly, $[Ca^{2+}]_N$ decayed more slowly than $[Ca^{2+}]_S$ (mono-exponential time constants of 6.1 and 2.5 s, respectively). After return of $[Ca^{2+}]$ to the prestimulatory level, a train of 10 stimuli was applied at a frequency of 1 Hz. The amplitude of the first $[Ca^{2+}]_S$ transient was 25% lower than that of the preceding single transient. Thereafter, $[Ca^{2+}]_S$ increased stepwise to a maximum that equalled that of the single transient. Similarly, the amplitude of the first $[Ca^{2+}]_N$ transient was 20% lower than that of the preceding single transient. In contrast to $[Ca^{2+}]_S$, $[Ca^{2+}]_N$ then increased to a maximum that was 2.3-fold higher than that of the single transient and equalled that of $[Ca^{2+}]_S$. In the nucleus, and to a lesser extent in the sarcoplasm, $[Ca^{2+}]$ decreased faster at the end of the stimulus train than after the preceding single stimulus (time constants of 3.3 and 2.1 s, respectively). To gain insight into the molecular principles underlying the shaping of the nuclear Ca^{2+} signal, a 3-D mathematical model was constructed. Intriguingly, quantitative modelling required the inclusion of a satiable nuclear Ca^{2+} buffer. Alterations in the concentration of this putative buffer had dramatic effects on the kinetics of the nuclear Ca^{2+} signal. This finding unveils a possible mechanism by which the skeletal muscle can adapt to changes in physiological demand.

Keywords: Electrical field stimulation; Human myotubes; Video-rate confocal imaging; Nuclear calcium handling; Mathematical modelling

1. Introduction

Many cells display complex patterns of intracellular Ca^{2+} signalling in response to an extracellular stimulus [1,2]. Most importantly, the spatial and temporal organization of these intracellular Ca^{2+} signals differs greatly between stimuli and cell types. Increasing evidence shows that these differences are accomplished by differential expression of the various components of the Ca^{2+}-signalling machinery [3]. This flexibility makes the intracellular Ca^{2+} signal particularly suitable for the regulatory control of a diverse array of cellular activities including fertilization, proliferation, development, contraction, secretion, learning and memory.

Intracellular Ca^{2+} signals originate at the plasma membrane and/or the endoplasmic reticulum by the opening of specific types of Ca^{2+} channels and subsequently spread throughout the cytoplasm [3]. Apart from altering the activi-

Abbreviations: $[Ca^{2+}]_S$, sarcoplasmic calcium concentration; $[Ca^{2+}]_N$, nuclear calcium concentration; ROI, region of interest; PMCA, plasma membrane calcium ATPase; SERCA, sarco/endoplasmic reticulum calcium ATPase; SR, sarcoplasmic reticulum; VOI, volume of interest; μ_S, μ_N, fitted mono-exponential time constant of Ca^{2+} removal in sarcoplasm and nucleus, respectively; $R_{max,S}$, $R_{max,S}$, peak Indo-1 ratio in the sarcoplasm and nucleus, respectively

* Corresponding author. Tel.: +31 24 3614589; fax: +31 24 3616413.
E-mail address: p.willems@ncmls.ru.nl (P.H.G.M. Willems).

0143-4160/$ – see front matter © 2005 Elsevier Ltd. All rights reserved.
doi:10.1016/j.ceca.2005.06.003

ties of cytoplasmic Ca^{2+} effector molecules, these cytoplasmic Ca^{2+} signals are also efficiently transmitted into the mitochondria and nucleus, where they control the rates of ATP production [4] and gene transcription [5], respectively.

Studies in recent years have identified Ca^{2+}-induced Ca^{2+}-release (CICR) as the underlying principle in the rapid propagation of cytoplasmic Ca^{2+} waves [2]. As far as mitochondrial Ca^{2+} uptake is concerned, evidence is now provided that this occurs through a highly selective Ca^{2+} channel present in the mitochondrial inner membrane [6]. On the other hand, there is an ongoing debate regarding the mechanism by which the cytoplasmic Ca^{2+} signal is transmitted into the nucleus.

Some evidence favours the idea that Ca^{2+} diffuses into the nucleoplasm through nuclear pores [7]. Other evidence, however, suggests that Ca^{2+} is released into the nucleoplasm through Ca^{2+} channels that are present in the inner nuclear membrane and opened by the action of inositol 1,4,5-trisphosphate (IP_3) [8]. In this respect, it is intriguing that in many cell types the nuclear envelope forms long, double-membraned extensions deep into the nucleus [9]. More recently, these extensions have been implicated in the IP_3-mediated release of Ca^{2+} in discrete areas of the nucleus [10]. Importantly, evidence has been provided that the IP_3-operated Ca^{2+} channels of these intranuclear extensions, or nucleoplasmic reticulum, are more sensitive to IP_3 than those of the endoplasmic reticulum, thus allowing independent regulation of nuclear and cytoplasmic Ca^{2+} [11]. Finally, recent data indicate that mitochondria readily move in and out of the lumen of the intranuclear extensions [12]. Because energized mitochondria rapidly accumulate large amounts of Ca^{2+}, disease-related disturbances of the energy state of these organelles will significantly alter the shape of the nuclear Ca^{2+} signal and thus affect transcription regulation.

Thus far, there is no evidence for the presence of intranuclear extensions in the nuclei of skeletal muscle fibres. On the other hand, IP_3 receptors were demonstrated to be preferentially present in the nuclear fraction of cultured rat myotubes [13]. Elevations in extracellular K^+ concentration were shown to cause a biphasic increase in intracellular Ca^{2+} concentration ($[Ca^{2+}]$). Detailed analysis revealed that the first increase was fast and associated with contraction, whereas the second increase, which was most prominent in the nuclei, was slow, mediated by IP_3 and responsible for the activation of the transcription factor CREB (cAMP response element-binding protein; [13–15]). Similarly, a Ca^{2+} ionophore, known to cause a sustained increase in intracellular $[Ca^{2+}]$, was found to increase the activity of the transcription factor NFAT (nuclear factor of activated T cells), in a primary culture of rabbit skeletal muscle [16,17]. The effect of the Ca^{2+} ionophore was mimicked by electrostimulation for 24 h [18].

In the latter study, measurement of the intracellular Ca^{2+} concentration revealed that this concentration invariably returned to the prestimulatory level in between the electrical stimuli. It should be noted, however, that the authors measured the average intracellular $[Ca^{2+}]$ of a single myotube. Therefore, sustained increases in nuclear Ca^{2+} concentration ($[Ca^{2+}]_N$), slightly higher than the prestimulatory level, might have been missed. In the present study we used video-rate UV confocal imaging and electrostimulation of cultured human skeletal myotubes to assess the relationship between the changes in $[Ca^{2+}]_S$ (sarcoplasmic Ca^{2+} concentration) and $[Ca^{2+}]_N$ during low- and high-frequency electrostimulation. The data presented show that $[Ca^{2+}]_N$ increased to significantly higher values upon changing from low- to high-frequency stimulation and quantitative modelling suggested an important role for nuclear Ca^{2+} buffering herein.

2. Materials and methods

2.1. Cell culture

Quadriceps needle muscle biopsies (25–50 mg) were obtained from healthy volunteers, as approved by the Dutch Committee on Medical Ethics. Myotube cultures were obtained as described previously [19]. In short, muscle samples were dissociated and incubated four times during 15 min in 20 ml Dulbecco's phosphate-buffered saline containing 30 mg trypsin, 15 mg collagenase and 15 mg albumin. Satellite cells were spun down at $50 \times g$, resuspended in Dulbecco's modified Eagle's medium (DMEM; Invitrogen, Breda, The Netherlands) supplemented with 20% (v/v) foetal calf serum (FCS; Integro, Zaandam, The Netherlands) and allowed to proliferate for 4–5 days. Aliquots of the primary culture were stored in liquid nitrogen. For each measurement, an aliquot was plated on glass cover slips and cultured to confluence in DMEM with 20% (v/v) FCS. One day after reaching confluence, the medium was replaced by DMEM supplemented with 0.4% (v/v) Ultroser G (Invitrogen) to promote myoblast fusion into myotubes.

2.2. Confocal Ca^{2+} measurements

Three to five days after induction of myoblast fusion, cover slips were washed with incubation medium (pH 7.4) containing 125 mM NaCl, 10 mM $NaHCO_3$, 1 mM NaH_2PO_4, 5 mM KCl, 2 mM $MgSO_4$, 1.8 mM $CaCl_2$, 10 mM HEPES and 10 mM glucose and cells were loaded with the ratiometric fluorescent Ca^{2+} indicator, Indo-1, in the presence of 10 μM Indo-1/AM (Molecular Probes) for 30 min at 37 °C. After loading, the cells were washed twice and incubated for an additional 15 min to remove excess dye and complete de-esterification. For acquisition of sarcoplasmic Ca^{2+} signals, cover slips were transferred to an incubation chamber (volume of 700 μl) mounted on the stage of an inverted microscope (Nikon Diaphot) attached to an OZ confocal unit (Noran Instruments, Naarden, The Netherlands) with a high-power argon ion laser (Coherent Enterprise, Santa Clara, CA, USA). Indo-1 was excited at 351 nm and emission light was

collected using a Nikon ×40 water immersion objective (NA 1.2) with high UV transmission. Emission light was separated by a 455 DCLP dichroic mirror (Chroma Technology Corp, Brattleboro, VT, USA), and quantified at 405 ± 45 nm and 485 ± 45 nm using two photomultipliers (Hamamatsu Photonics Kabushiki Gaisha, Japan). The confocal slit was chosen to give an axial resolution of 10 μm [20]. With this setting a workable signal-to-noise ratio at minimal laser intensity was achieved (output of 15 mW, equivalent to 28 μW at the back of the objective lens; [21]). Basal ratio signals were stable and no UV-induced deterioration of cells was observed during the measurements. The OZ hardware was controlled by the Intervision acquisition software (version 1.5, Noran Instruments) running under IRIX 6.5 on an Indy workstation (Silicon Graphics Inc., Mountain View, CA, USA) equipped with 256 Mb of internal memory. Before starting the measurement, regions of interest (ROIs) were indicated in sarcoplasm and nucleus of the myotube. For background correction, an additional ROI was situated outside the myotube. During the measurement, the average fluorescence emission intensities from each ROI were calculated and individually stored in ASCII format for off-line background correction and ratioing.

2.3. Electrical field stimulation

For electrical stimulation we used a method described earlier [21–23]. In short, two platinum electrodes were fixed to opposite sites of the chamber and connected to a Grass SD9 stimulator. Myotubes were stimulated (10 ms, 16 V) at the frequencies indicated. All recordings were performed at room temperature.

2.4. Immunocytochemistry

Three to five days after induction of myoblast fusion, cover slips were washed three times with phosphate-buffered saline (PBS), air-dried, and stored at −70 °C. After rehydration in PBS, PBS containing 1% (w/v) BSA was added followed by incubation with rabbit anti-sarcoplasmic reticulum Ca^{2+}-ATPase antibody (a kind gift from Dr. J. Timmermans, Department of Cell Physiology, Radboud University Medical Center Nijmegen, The Netherlands) for 90 min. After washing in PBS, cells were incubated with Alexa 488-conjugated goat anti-rabbit IgG (Molecular Probes Inc., Leiden, The Netherlands). Cover slips were mounted in Mowiol for immunolocalization on a Zeiss Axioskop photomicroscope (Carl Zeiss, Oberkochen, Germany).

2.5. Data analysis and mathematical modelling

Experimental data (ASCII format) were imported into Origin Pro 6.1 (OriginLabs, Northampton, MA, USA) for off-line analysis and visualization. Emission signals were background-corrected before the fluorescence emission ratio (405/485 nm) was calculated. For quantitative analysis, the prestimulatory ratio was normalized to 1 and the amplitude of an electrically induced $[Ca^{2+}]$ increase was expressed as the peak ratio (R_{max}) minus 1. Data are presented as mean ± standard error (S.E.M.) unless stated otherwise. Parameters obtained from curve fitting are given as mean ± standard deviation (S.D.). Mathematical modelling was performed with MATLAB 6.1 (The Mathworks Inc., Natick, MA, USA) using custom scripts.

3. Results

3.1. $[Ca^{2+}]$ dynamics in sarcoplasm and nucleus following a single stimulus

In contrast to mouse myotubes and C2C12 cells [22,23], human myotubes did not display spontaneous $[Ca^{2+}]$ rises [21]. In previous work, we used elevations in extracellular $[K^+]$ to increase $[Ca^{2+}]$ in human myotubes [24]. However, this method does not allow high-frequency stimulation. Therefore, electrical field stimulation was applied in a more recent study [21]. It was found that electrically induced $[Ca^{2+}]$ rises occurred only in myotubes and not in myoblasts.

Here, we combined video-rate UV confocal imaging and electrostimulation to assess the relationship between the changes in $[Ca^{2+}]_S$ and $[Ca^{2+}]_N$ during low and high-frequency stimulation of human myotubes. Three to five days after induction of myoblast fusion, cells were loaded with the ratiometric UV Ca^{2+}-indicator Indo-1. Myotubes were readily recognized by virtue of their elongated shape and the presence of multiple nuclei (Fig. 1A; left panel). Importantly, ratio images of unstimulated myotubes revealed no spatial differences in ratio signal (Fig. 1A; right panel and trace to the right). Fig. 1B shows that a single electrical stimulus (10 ms, 16 V) readily increased $[Ca^{2+}]$ in two ROIs, a sarcoplasmic one and a nuclear one, located in close proximity to each other (Fig. 1A; left panel). Within the time resolution of the measurement (33 ms), the onset of the $[Ca^{2+}]$ rise was the same in both compartments. However, the maximal rate of $[Ca^{2+}]$ rise was significantly lower in the nucleus (rising speeds of 3.1 and 11.3 ratio units/s for $[Ca^{2+}]_N$ and $[Ca^{2+}]_S$, respectively). In both compartments, the peak $[Ca^{2+}]$ was reached within 100 ms, after which $[Ca^{2+}]$ gradually declined to the prestimulatory level (Fig. 1C; left panel). The peak $[Ca^{2+}]$, or amplitude, was significantly lower in the nucleus (0.29 ± 0.02 and 0.70 ± 0.05 ratio units for $[Ca^{2+}]_N$ and $[Ca^{2+}]_S$, respectively) (Fig. 1D; column marked 'single'). In both compartments, the decay phase of the $[Ca^{2+}]$ transient was adequately described by a mono-exponential function ($R(t) = R_{max}e^{-t/\mu} + 1$; $R^2 > 0.90$), indicating the involvement of a single Ca^{2+} removal process [21,25,26]. The time constant (μ) of the decay phase was significantly higher for the nucleus (μ values of 6.11 ± 0.30 s and 2.5 ± 0.15 s for $[Ca^{2+}]_N$ and $[Ca^{2+}]_S$, respectively), indicating that Ca^{2+} was less rapidly removed from this organelle (Fig. 1E; column marked 'single').

3.2. Frequency dependence of sarcoplasmic and nuclear $[Ca^{2+}]$ changes

To determine the dependence of the kinetics of the sarcoplasmic and nuclear $[Ca^{2+}]$ rises on stimulus frequency, we used a protocol consisting of a single stimulus followed by two trains of 10 stimuli, a first one at 1 Hz and a second one at 2 Hz (Fig. 1C). In between, $[Ca^{2+}]$ was allowed to return to the prestimulatory level (dashed line). The peak value of the first $[Ca^{2+}]_S$ rise during the 1 Hz stimulus train was 25% lower than that of the preceding single $[Ca^{2+}]_S$ transient (Fig. 1C; arrows with open heads in left and middle

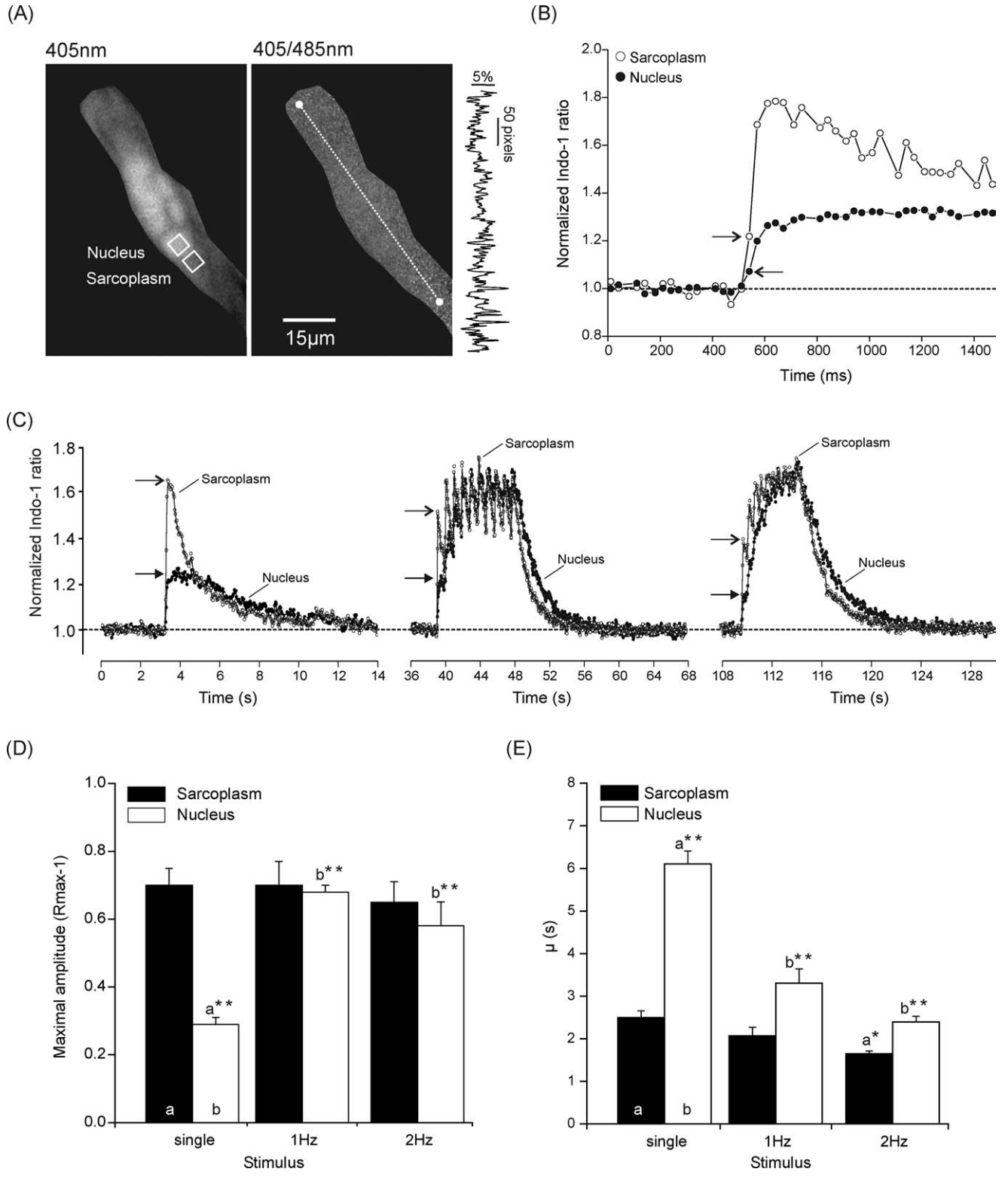

panel). During 1 and 2 Hz stimulation, $[Ca^{2+}]_S$ did not return to the prestimulatory level in between the stimuli and the peak value increased stepwise to a maximum, reached after three consecutive stimuli, that equalled that of the preceding single transient (0.70 ± 0.07 and 0.70 ± 0.05 ratio units, respectively) (Fig. 1D). Similarly, the peak value of the first $[Ca^{2+}]_N$ rise was 20% lower than that of the preceding single $[Ca^{2+}]_N$ transient (Fig. 1C; arrows with filled heads). In this compartment, however, the peak value increased stepwise to a maximum, reached after seven to eight consecutive stimuli, that was 2.3-fold higher than that of the preceding single transient (0.68 ± 0.02 and 0.29 ± 0.02 ratio units, respectively) and equalled that of $[Ca^{2+}]_S$. In the nucleus, $[Ca^{2+}]$ decreased faster at the end of the stimulus train than during the preceding single transient (time constants of 3.30 ± 0.34 s and 6.11 ± 0.30 s, respectively) (Fig. 1E). The same was observed for the sarcoplasm (time constants of 2.07 ± 0.19 s and 2.50 ± 0.15 s for the $[Ca^{2+}]$ decay at the end of the first stimulus train and after the preceding single stimulus, respectively). The reduction in time constant for the decrease in $[Ca^{2+}]_S$ and $[Ca^{2+}]_N$ amounted to 17 and 46%, respectively.

After return of $[Ca^{2+}]$ to the prestimulatory level, a 2 Hz stimulus train was applied. Now, the peak value of the first $[Ca^{2+}]_S$ rise was 40% lower than that of the initial single $[Ca^{2+}]_S$ transient (Fig. 1C; arrows with open heads in left and right panel). However, upon repeated stimulation this value increased stepwise to a maximum, reached after five consecutive stimuli, that was not statistically different from that of the initial single transient (0.65 ± 0.06 and 0.70 ± 0.05 ratio units, respectively) (Fig. 1D). Similarly, the peak value of the first $[Ca^{2+}]_N$ rise was 41% lower than that of the initial single $[Ca^{2+}]_N$ transient (Fig. 1C; arrows with filled heads in left and right panel). Again, the peak value increased stepwise to a maximum, reached after 9–10 consecutive stimuli, that was markedly (2.0-fold) higher than that of the initial single transient (0.58 ± 0.07 and 0.29 ± 0.02 ratio units, respectively) and virtually equalled that of $[Ca^{2+}]_S$. In both compartments, the rate of $[Ca^{2+}]$ decay was faster at the end of the 2 Hz stimulus train than at the end of the preceding 1 Hz stimulus train (time constants of 1.65 ± 0.05 s and 2.07 ± 0.19 s for the sarcoplasm and 2.40 ± 0.13 s and 3.30 ± 0.34 s for the nucleus, respectively) (Fig. 1E). Compared to the initial single stimulus, the reduction in time constant amounted to 34 and 61% for the decrease in $[Ca^{2+}]_S$ and $[Ca^{2+}]_N$, respectively. For both sarcoplasm and nucleus the Indo-1 emissions at 405 and 485 nm were linearly correlated ($p < 0.001$). The fitted lines were virtually parallel, indicating that Indo-1 behaved the same in both cellular compartments (data not shown).

3.3. Three-dimensional model for amplitude modulation of nuclear Ca^{2+} signals

To gain insight into the molecular principles underlying the shaping of the nuclear Ca^{2+} signal, we developed a 3-D mathematical model using a minimal number of components required to quantitatively reproduce the experimental findings. The numerical data presented in Fig. 1D and E were obtained from equally sized ROIs located in close proximity to each other in the nuclear and sarcoplasmic compartment (Fig. 1A, left panel). The nuclear ROI consisted of a square, whose corners touched the boundary of the organelle (Fig. 2A). The lateral dimensions of this square were $10\,\mu m \times 10\,\mu m$. A square with identical dimensions was drawn in the sarcoplasm. Because the confocal slit was chosen to give an axial section thickness of $10\,\mu m$ [20], this means that fluorescence light was sampled from two cubical volumes of interest (VOIs) with a side of $10\,\mu m$ (Fig. 2B). Geometrically, the nucleus was considered as a 3-D sphere, consisting of five concentric shells surrounded by five shells of sarcoplasm (Fig. 2C; grey area; projection on x–y plane shown). Shells were $1.5\,\mu m$ apart and used to calculate $[Ca^{2+}](x, y, z, t)$. For calculation of $[Ca^{2+}]_S(t)$ and $[Ca^{2+}]_N(t)$ the experimental geometry was accounted for by calculating $[Ca^{2+}](x, y, z, t)$, representing the concentration of Ca^{2+} at position (x, y, z) at time t, from the full 3-D multi-shell model followed by integration across the corresponding VOI (using appropriate boundary conditions).

Earlier studies demonstrated that during each electrical stimulus a constant fraction α of the Ca^{2+} in the SR is released and that this fraction decreases with increasing stimulus intensity [27,28]. This is reflected in our model by using $\alpha = 0.5$ for a single stimulus, $\alpha = 0.4$ for a 1 Hz stimulus and $\alpha = 0.25$ for a 2 Hz stimulus.

Previous work in rat soleus muscle revealed a perinuclear localization of the sarcoplasmic reticulum, suggesting a high

Fig. 1. Sarcoplasmic and nuclear calcium changes induced by low and high-frequency electrical field stimulation. (A) Confocal image of a human skeletal myotube loaded with the ratiometric Ca^{2+} indicator Indo-1. The left panel shows a 405 nm image in which a single myotube was highlighted using a mask. Several nuclei can be distinguished (high fluorescence signal). Two regions of interest (ROIs), one in the sarcoplasm and another in nucleus are indicated (squares). Analysis of the Indo-1 ratio signal across the myotube (right panel; dotted line) did not reveal spatial differences (vertical trace). (B) Typical example of a Ca^{2+} transient induced by a single electrical stimulus. The time of onset of the sarcoplasmic (open circles) and nuclear $[Ca^{2+}]$ signal (filled circles) was identical (arrows) but the latter displayed a reduced rate of increase and maximal amplitude. (C) Ca^{2+} kinetics in the sarcoplasm (open symbols) and nucleus (filled symbols) of the same myotube during a single, 1 and 2 Hz electrical field stimulation. The dashed line represents basal $[Ca^{2+}]$. Open and filled arrows indicate a reduction in amplitude of the first Ca^{2+} transient at higher stimulus frequency in the sarcoplasm and nucleus, respectively. (D) Quantitative analysis of the maximal amplitude of sarcoplasmic (filled bars) and nuclear Ca^{2+} signals (open bars) for electrical stimuli of increasing frequency. Because all traces were normalized to one, the maximal amplitude was calculated from $(R_{max} - 1)$, with R_{max} being the maximal Indo-1 ratio reached. (E) Similar to (D) but now for the time constant (μ) of a mono-exponential function ($R(t) = R_{max}e^{-t/\mu} + 1$) fitted to the decay of the Ca^{2+} transients. Of note, a lower μ indicates a faster decay in $[Ca^{2+}]$. $^{*}p < 0.05$ and $^{**}p < 0.01$ designate a significant difference with the indicated column. Data was obtained from nine myotubes (24 transients) for the single stimulus, and five myotubes (five transients) for 1 and 2 Hz stimulation.

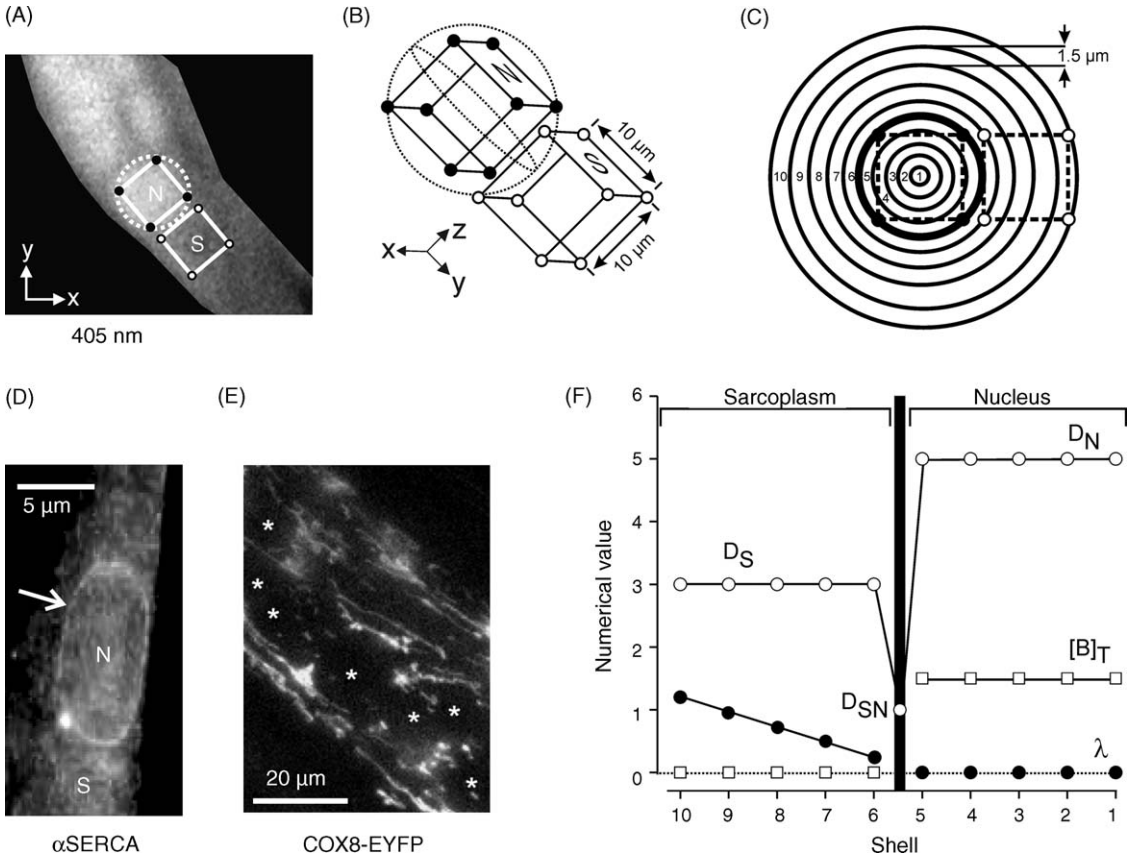

Fig. 2. Construction of a 3-D mathematical model. (A) Magnification of the left panel of Fig. 1A showing the location of the sarcoplasmic (S) and nucleoplasmic (N) ROIs. (B) 3-D geometry of the ROIs, accounting for their square lateral dimensions of 10 μm and an optical plane thickness of 10 μm. Fluorescence is sampled from two cubic volumes of interest in the sarcoplasm (open circles) and nucleus (filled circles). (C) 2-D projection of the 3-D model consisting of 10 concentric shells placed 1.5 μm apart. Shells 1–5 and 6–10 correspond to the nucleus and sarcoplasm, respectively. The squares reflect the ROIs and VOIs in (A) and (B). The boundary between sarcoplasm and nucleus is represented by the black circle. (D) Immunocytochemical localization of SERCA pumps demonstrating their perinuclear localization (arrow). (E) Living human skeletal myotubes expressing a mitochondria-targeted variant of yellow fluorescent protein (COX8-EYFP). Nuclei are marked with asterisks. No perinuclear clustering of mitochondria was observed. (F) Numerical values of parameters in the different shells of the optimal 3-D model (see Section 3). D_S and D_N (open circles) are the Ca^{2+} diffusion constants ($\mu m^2/s$) in the sarcoplasm and nucleus, respectively. D_{SN} represents the lower Ca^{2+} diffusion constant ($\mu m^2/s$) at the boundary (thick black line) between sarcoplasm and nucleus. Squares indicate the value of $[B]_T$, the total buffer concentration (μM) in the nucleus, and λ (filled circles) depicts the mono-exponential time constant (s) of Ca^{2+} removal. $[B]_T$ and λ were zero (dotted line) in the sarcoplasm and nucleus, respectively (see Section 3 for details).

abundance of SERCA pumps in this region [29–31]. Immunocytochemical analysis confirmed that this was also the case for the human myotubes used in this study (Fig. 2D; arrow). Therefore, the Ca^{2+} removal rate was considered to be highest around the nucleus and to decrease linearly with the distance from the nuclear membrane. This was accounted for in the model by a decrease in λ, the first-order time constant that governs the process of Ca^{2+} removal, from 1.2 to 0.24 s when going from shell 10 to shell 6 (Fig. 2F, filled circles). Under all conditions, the rate of Ca^{2+} removal in the sarcoplasm exceeded that in the nucleus. This suggests that the rate of Ca^{2+} removal from the nucleus is determined by that in the sarcoplasm. Therefore, our model does not include active Ca^{2+} removal in the nucleus. Consequently, λ was set to zero in the nucleus (shells 1–5). It was further assumed that Ca^{2+} diffusion in the nucleus was somewhat faster than in the sarcoplasm ($D_N = 5.0\ \mu m^2/s$, $D_S = 3.0\ \mu m^2/s$).

Because strategically localized mitochondria have dramatic effects on the propagation of intracellular Ca^{2+} signals [32,33], we determined their subcellular localization by expressing a mitochondria-targeted variant of yellow fluorescent protein (COX8-EYFP) using a transfection method described previously [34]. Fig. 2E (asterisks indicate nuclei) shows the absence of a clear perinuclear clustering of these organelles in human skeletal myotubes. Similar results were obtained with JC-1 (5,5′,6,6′-tetrachloro-1,1′,3,3′-tetraethylbenzimidazolylcarbocyanine iodide), a cationic dye that accumulates in mitochondria (not shown). These findings make it unlikely that mitochondria form an effective barrier for the sarcoplasmic Ca^{2+} signal to propagate into the nucleus.

In agreement with earlier findings, the nuclear membrane was considered to be semi-permeable for Ca^{2+} [31,35–37]. Mathematically, this was achieved by using a reduced Ca^{2+}

diffusion constant (D_{SN}) of 1.0 μm^2/s between the sarcoplasm and nucleus (i.e. between shells 5 and 6; Fig. 2F; open circles). Considering the above assumptions, the Ca^{2+} flux in the nucleus (J_N) is entirely driven by diffusion:

$$J_N(x, y, z, t) = -D_N \nabla C(x, y, z, t) \quad (1)$$

On its turn, the Ca^{2+} flux in the sarcoplasm (J_S) is determined by Ca^{2+} release, diffusion and extrusion:

$$J_S(x, y, z, t) = \text{release} - D_S \nabla C(x, y, z, t) - \text{extrusion} \quad (2)$$

The continuity equation, stating that the total amount of Ca^{2+} is preserved, gives:

$$-\frac{\partial C(x, y, z, t)}{\partial t} = \frac{\partial j(x, y, z, t)}{\partial x} + \frac{\partial j(x, y, z, t)}{\partial y} + \frac{\partial j(x, y, z, t)}{\partial z} \quad (3)$$

Substitution of j in Eqs. (1) and (2) in Eq. (4) gives the diffusion equation:

$$\frac{\partial C(x, y, z, t)}{\partial t} = D\left\{\frac{\partial^2 C(x, y, z, t)}{\partial x^2} + \frac{\partial^2 C(x, y, z, t)}{\partial y^2} + \frac{\partial^2 C(x, y, z, t)}{\partial z^2}\right\} \quad (4)$$

Due to symmetry this equation can be expressed in spherical coordinates:

$$\frac{\partial C(r, t)}{\partial t} = D\left\{\frac{\partial^2 C(r, t)}{\partial r^2} + \frac{2}{r}\frac{\partial C(r, t)}{\partial r}\right\} \quad (5)$$

To simulate an electrical stimulus, $[Ca^{2+}]_S$ was increased within a single time step (1 ms) to 1 μM, a concentration typical for skeletal muscle [38]. The set of Eqs. (1)–(5) was solved using Newton-integration.

3.4. Quantitative modelling requires nuclear Ca^{2+} buffering

During experiments the ratio between the sarcoplasmic and nuclear peak $[Ca^{2+}]$ ($R_{max,S}/R_{max,N}$) declined from

Table 1
Quantitative comparison between experimental data and mathematical model

	Single stimulus			1 Hz stimulus			2 Hz stimulus		
	$R_{max,S}$	$R_{max,N}$	$R_{max,S}/R_{max,N}$	$R_{max,S}$	$R_{max,N}$	$R_{max,S}/R_{max,N}$	$R_{max,S}$	$R_{max,N}$	$R_{max,S}/R_{max,N}$
Experiment	0.70 ± 0.05	0.29 ± 0.02	2.41 (100%)	0.70 ± 0.07	0.68 ± 0.02	1.03 (43%)	0.65 ± 0.06	0.58 ± 0.07	1.12 (46%)
Model									
+BUFFER, D_{SN} = 0.5	0.66 μM	0.15 μM	4.40 (100%)	0.76 μM	0.55 μM	1.38 (31%)	0.76 μM	0.60 μM	1.27 (29%)
+BUFFER, D_{SN} = 1.0	0.66 μM	0.20 μM	3.30 (100%)	0.77 μM	0.57 μM	1.35 (41%)	0.77 μM	0.65 μM	1.18 (36%)
+BUFFER, D_{SN} = 2.8	0.66 μM	0.25 μM	2.64 (100%)	0.77 μM	0.58 μM	1.32 (50%)	0.78 μM	0.67 μM	1.16 (44%)
+BUFFER, D_{SN} = 3.0	0.66 μM	0.25 μM	2.64 (100%)	0.80 μM	0.58 μM	1.40 (52%)	0.78 μM	0.67 μM	1.16 (44%)
−BUFFER, D_{SN} = 0.5	0.66 μM	0.36 μM	1.83 (100%)	0.76 μM	0.56 μM	1.36 (74%)	0.78 μM	0.66 μM	1.18 (65%)
−BUFFER, D_{SN} = 1.0	0.66 μM	0.40 μM	1.65 (100%)	0.77 μM	0.58 μM	1.33 (81%)	0.78 μM	0.67 μM	1.16 (70%)
−BUFFER, D_{SN} = 2.8	0.66 μM	0.43 μM	1.53 (100%)	0.77 μM	0.59 μM	1.31 (86%)	0.78 μM	0.68 μM	1.15 (75%)
−BUFFER, D_{SN} = 3.0	0.66 μM	0.43 μM	1.53 (100%)	0.77 μM	0.59 μM	1.31 (86%)	0.78 μM	0.68 μM	1.15 (75%)

	Single stimulus			1 Hz stimulus			2 Hz stimulus		
	μ_S	μ_N	μ_N/μ_S	μ_S	μ_N	μ_N/μ_S	μ_S	μ_N	μ_N/μ_S
Experiment	2.5 ± 0.15	6.1 ± 0.3	2.40 (100%)	2.1 ± 0.19	3.3 ± 0.34	1.60 (67%)	1.70 ± 0.05	2.4 ± 0.13	1.40 (58%)
Model									
+BUFFER, D_{SN} = 0.5	1.25 s	4.47 s	3.58 (100%)	1.39 s	2.12 s	1.52 (42%)	1.36 s	2.11 s	1.55 (43%)
+BUFFER, D_{SN} = 1.0	1.31 s	3.28 s	2.50 (100%)	1.39 s	2.21 s	1.58 (63%)	1.37 s	2.09 s	1.53 (61%)
+BUFFER, D_{SN} = 2.8	1.39 s	2.54 s	1.83 (100%)	1.38 s	1.97 s	1.43 (78%)	1.37 s	1.64 s	1.20 (66%)
+BUFFER, D_{SN} = 3.0	1.39 s	2.56 s	1.80 (100%)	1.39 s	1.86 s	1.33 (74%)	1.32 s	1.80 s	1.36 (76%)
−BUFFER, D_{SN} = 0.5	1.30 s	1.36 s	1.05 (100%)	1.24 s	1.31 s	1.06 (101%)	1.24 s	1.37 s	1.10 (105%)
−BUFFER, D_{SN} = 1.0	1.32 s	1.29 s	1.02 (100%)	1.23 s	1.25 s	1.02 (100%)	1.23 s	1.27 s	1.03 (101%)
−BUFFER, D_{SN} = 2.8	1.33 s	1.26 s	1.06 (100%)	1.22 s	1.25 s	1.02 (96%)	1.23 s	1.24 s	1.01 (95%)
−BUFFER, D_{SN} = 3.0	1.34 s	1.25 s	1.07 (100%)	1.21 s	1.23 s	1.02 (95%)	1.22 s	1.22 s	1.00 (93%)

Experimental data was normalized to basal levels after which the maximal amplitude of the Ca^{2+} signal was calculated by subtracting one from the maximal Indo-1 ratio ($R_{max} - 1$). Of note, model data did not require this correction of R_{max}. μ_S and μ_N are exponential time constants that were obtained by fitting a mono-exponential function to the decay phase of the experimental and simulated data. Experimental data was obtained from nine myotubes (24 transients) for the single stimulus, and five myotubes (five transients) for 1 and 2 Hz stimulation. Relative changes in R_{max} and μ between sarcoplasm and nucleus are given by $R_{max,S}/R_{max,N}$ and μ_N/μ_S and expressed as percentage of these ratios for a single stimulus. Simulation parameters: α = 0.5 (single stimulus), 0.4 (1 Hz stimulus) or 0.25 (2 Hz stimulus), D_N = 5.0 μm^2/s, D_S = 3.0 μm^2/s, D_{SN} = variable (see table, unit: μm^2/s), $[B]_T$ = 1.5 μM (+BUFFER) or 0.0 μM (−BUFFER), λ = 1.2 s (see Section 3 for details).

2.41 (100%) for the single transient, to 1.03 (43%) for the 1 Hz stimulus train and 1.12 (46%) for the 2 Hz stimulus train (Table 1). In the model (marked: −BUFFER, $D_{SN} = 1.0$), these ratios were 1.65 (100%), 1.33 (81%) and 1.16 (70%), respectively. Similarly, the ratio between the experimentally determined time constants for the decay of $[Ca^{2+}]_N$ and $[Ca^{2+}]_S$ (μ_N/μ_S) was 2.40 (100%) for the single transient, 1.60 (67%) for the 1 Hz stimulus train and 1.40 (58%) for the 2 Hz stimulus train, whereas in the model (−BUFFER, $D_{SN} = 1.0$) these ratios were 1.02 (100%), 1.02 (100%) and 1.03 (101%), respectively. These findings demonstrate that (I) the model was able to qualitatively predict the amplitude reduction in $[Ca^{2+}]_N$, as a function of electrostimulation frequency, but (II) failed to reproduce the differences in μ_N and μ_S observed during experiments.

The quantitative performance of the model was considerable improved by introducing an immobile Ca^{2+} buffer B in the nuclear shells at a total concentration ($[B]_T$) of 1.5 μM (Fig. 2F, open squares). The buffer was assumed to display first order reaction kinetics, which was accounted for by adding $d[BCa^{2+}]/dt = K_{on}[B][Ca^{2+}]_N - K_{off}[BCa^{2+}]$ to the right hand side of Eq. (1), with $K_{on} = 4\ \mu M/s$, $K_{off} = 0.5\ s^{-1}$ and $K_d = K_{off}/K_{on} = 0.125\ \mu M$. Models including this nuclear buffer (+BUFFER), predicted the stimulus-dependent decrease in $R_{max,S}/R_{max,N}$ and μ_N/μ_S much better than those without nuclear buffer (−BUFFER), irrespective of the value of D_{SN} (Fig. 3A and B and Table 1). The best fit between experiment and model was obtained using $[B]_T = 1.5\ \mu M$ and $D_{SN} = 1\ \mu m^2/s$ (Fig. 3C). The latter value reflects a three-fold reduction in Ca^{2+} diffusion (from $D_S = 3\ \mu m^2/s$ to $D_{SN} = 1\ \mu m^2/s$) upon crossing the boundary between sarcoplasm and nucleus (Fig. 2F). In agreement with the experimental findings (Fig. 1C), simulations predicted a decrease in amplitude of $[Ca^{2+}]_S$ and $[Ca^{2+}]_N$ for the first stimulus at 1 and 2 Hz stimulation (Fig. 3C; arrows with open and filled heads).

Magnification of the rising phase of the single first transient (Fig. 3D) revealed that, in agreement with experiments (Fig. 1B), $[Ca^{2+}]_S$ increased faster than $[Ca^{2+}]_N$. Moreover, changes in D_{SN} did not affect the time of onset of the nuclear Ca^{2+} signal, slightly altered the kinetics of $[Ca^{2+}]_S$, but reduced the amplitude and decay rate of $[Ca^{2+}]_N$.

Because quantitative modelling required nuclear Ca^{2+} buffering, we performed additional simulations to determine how this buffer might contribute to the decrease in amplitude of $[Ca^{2+}]_N$ at higher stimulus frequency. Plotting $[B]_N$, the concentration of free Ca^{2+} buffer in the nucleus, during different stimulation regimes revealed a large reduction in $[B]_N$ at 1 and 2 Hz stimulation (Fig. 3E). This means that the nuclear Ca^{2+} buffer becomes increasingly saturated as a function of stimulation intensity. The saturation effect was quantitatively similar during simulations with increased or decreased values of D_{SN}.

4. Discussion

Video-rate confocal microscopy of fura-2-loaded human skeletal myotubes was used to gain insight into the temporal and quantitative relationship between the sarcoplasmic and nuclear Ca^{2+} concentration changes following electrical stimulation. Each stimulus evoked a transient increase in $[Ca^{2+}]_S$ and $[Ca^{2+}]_N$ and it was observed that $[Ca^{2+}]_N$, but not $[Ca^{2+}]_S$, reached a considerably higher value during repetitive $[Ca^{2+}]_S$ transients as compared to a single $[Ca^{2+}]_S$ transient. Using quantitative mathematical modelling we investigated the involvement of semi-permeability of the nuclear membrane, inhomogeneous sarcoplasmic Ca^{2+} pumping and high-affinity nuclear Ca^{2+} buffering in this amplitude modulation (AM).

4.1. Validation of the use of Indo-1 to monitor electrically evoked changes in $[Ca^{2+}]$

It was observed that Indo-1 emission signals (especially at 405 nm) were higher in the nucleus than in the sarcoplasm. This property allowed precise identification of sarcoplasmic and nuclear ROIs. Importantly, unstimulated myotubes displayed no spatial differences in Indo-1 ratio. This excludes the presence of a standing gradient between $[Ca^{2+}]_S$ and $[Ca^{2+}]_N$ and makes it unlikely that our results are biased by dye compartmentalization. Others have found that steady-state Indo-1 ratios, in contrast to Fluo-3 signals, were insensitive to pH, temperature and dye concentration and did not differ between cytosol and nucleoplasm for Ca^{2+} concentrations ranging from 10 to 10000 nM [39]. Therefore, we conclude that the observed kinetic differences between $[Ca^{2+}]_S$ and $[Ca^{2+}]_N$ are unlikely to reflect Indo-1 associated artefacts.

4.2. A 3-D model for amplitude modulation of nuclear Ca^{2+} signals

When comparing the sarcoplasmic and nuclear Ca^{2+} changes evoked by a single electrical stimulus with those evoked by a subsequent train of stimuli at a frequency of 1 Hz, two major differences were observed. First, $[Ca^{2+}]_N$ stepwise increased to a value that was 2.3-fold higher than following a single stimulus, whereas the maximum value of $[Ca^{2+}]_S$ remained the same. To better understand the mechanism underlying this frequency-dependent AM of $[Ca^{2+}]_N$, a 3-D mathematical model was developed from which data were sampled in agreement with the experimental geometry. In our model, each electrical stimulus was simulated by an instantaneous (within 1 ms) increase of $[Ca^{2+}]_S$ to 1 μM. This direct coupling reflects the highly efficient physical interaction between the dihydropyridine receptor (DHPR) voltage sensor and the ryanodine-sensitive Ca^{2+} release channel (RyR) on the sarcoplasmic reticulum (SR; [38]). Second, the amplitude of the first $[Ca^{2+}]_S$ transient of the 1 Hz train was 25% lower than that of the preceding single $[Ca^{2+}]_S$ transient, whereas that of the subsequent 2 Hz train was even

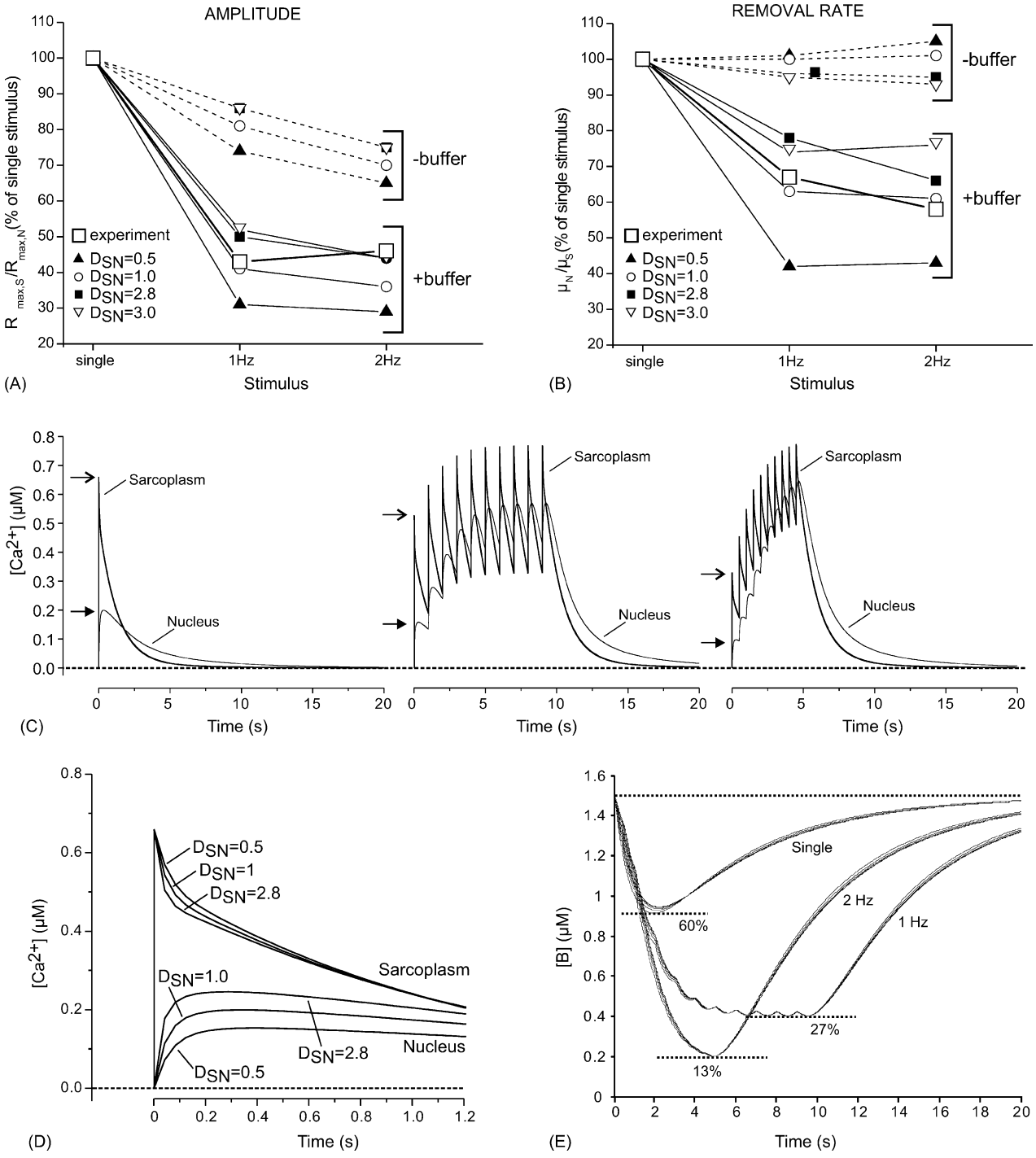

Fig. 3. Modeling of sarcoplasmic and nuclear calcium changes during electrical field stimulation. (A) Ratio between the maximal amplitude of the nuclear and sarcoplasmic Ca^{2+} signal, calculated from the ratio between the maximal Indo-1 ratio in nucleus and sarcoplasm ($R_{max,S}/R_{max,N}$), for stimuli of increasing frequency. The open square represents experimental data whereas the other symbols indicate model simulations for different values of D_{SN} ($\mu m^2/s$), the Ca^{2+} diffusion coefficient at the boundary between sarcoplasm and nucleus. Experimental data was normalized to one and therefore the ratio was calculated from $(R_{max,S}-1)/(R_{max,N}-1)$. Ratios for the 1 and 2 Hz stimulus were expressed as percentage of the ratio for a single stimulus (data from Table 1). Inclusion of a nuclear Ca^{2+} buffer (+BUFFER) was required for quantitative simulation of the experimental results. (B) Similar to (A) but now for μ_N/μ_S, the ratio between the mono-exponential time constant of Ca^{2+} in nucleus and sarcoplasm. Nuclear Ca^{2+} buffering was required for quantitative simulation. (C) Simulated experiment for a model with nuclear Ca^{2+} buffering ($[B]_T = 1.5\ \mu M$) and a reduced Ca^{2+} diffusion across the nuclear membrane ($D_{SN} = 1.0\ \mu m^2/s$). Open and filled arrows indicate a reduction in amplitude of the first Ca^{2+} transient at higher stimulus frequency in the sarcoplasm and nucleus, respectively. The latter was also observed during experiments. Simulation parameters can be found in Table 1 and details are in the Section 3. (D) Magnification of the rising phase of the transient in the left panel of (C) for different values of D_{SN}. Simulated traces were down sampled to 30 Hz to allow faithful comparison with experiments. (E) Time course of the concentration of free nuclear Ca^{2+} buffer [B] during a single, 1 and 2 Hz stimulus. For details see Section 3.

40% lower. This indicates that the amplitude of an electrically evoked $[Ca^{2+}]_S$ transient depends on whether or not a myotube is stimulated before. This phenomenon can be explained in several ways. For instance, the filling state of the SR might be decreased as a consequence of prior stimulation. Another possibility is that the DHPR and/or RyR are desensitized as a consequence of prior stimulation. In this context, it has been found that inorganic phosphate exerts a negative feedback on the RyR [27,28]. To account for the observed decrease in amplitude when going from the initial single stimulus to the first $[Ca^{2+}]_S$ transient of the 1 Hz pulse train and subsequent 2 Hz pulse train, we included a term α in our mathematical model. The lower the value of α, the less Ca^{2+} is released during each electrical stimulus. For an optimal fit of the experimental data, values of α of 0.5, 0.4 and 0.25 were required for the initial single stimulus and the first (1 Hz) and second (2 Hz) pulse train, respectively. With these values of α, the model not only reproduced the progressive decrease in amplitude of the first Ca^{2+} transient of the two stimulus trains but also the maximal $[Ca^{2+}]_S$ reached during the successive stimulations. In other words, when α was kept constant (for instance 0.5), the amplitude of the first Ca^{2+} transient of each of the two stimulus trains was the same as that of the initial single stimulus, whereas the maximal amplitude reached during each of the stimulus trains was significantly higher than that of the initial single stimulus.

Immunocytochemistry revealed a preferential perinuclear staining for SERCA pumps. Similar results were obtained with cardiomyocytes [40] and coronary smooth muscle cells [41]. Therefore in the model, sarcoplasmic Ca^{2+} removal (accounted for by a single time constant λ) was considered to be inhomogeneous, being highest just outside the nucleus. Quantitative simulations required a value of $\lambda = 1.2$ s, in close agreement with experimental findings. Under all conditions, Ca^{2+} removal was faster in the sarcoplasm as compared to the nucleus. This suggests that the rate of sarcoplasmic Ca^{2+} removal determines the Ca^{2+} removal rate in the nucleus. This finding supports the idea that Ca^{2+} removal from the nucleus does not involve the action of Ca^{2+}-ATPases and/or Ca^{2+}-exchangers on the inner membrane of the nuclear envelope but rather reflects the diffusion of Ca^{2+} from the nucleoplasm via nuclear pore complexes (NPCs) into the sarcoplasm [35,36,42]. Based on these considerations, we modelled a first-order Ca^{2+} removal process only in the sarcoplasm and not in the nucleus.

Skeletal myotubes are densely packed with mitochondria arranged in rows along the length of the cell [43]. Mitochondria can accumulate significant amounts of Ca^{2+} thereby changing the spatio-temporal kinetics of the intracellular Ca^{2+} signal. The present finding that the maximal increase in $[Ca^{2+}]_S$ was not different between the pulse trains and the preceding single stimulus suggests that mitochondrial Ca^{2+} buffering was already maximal during the single stimulus and can therefore not be responsible for the lower increase in $[Ca^{2+}]_N$ during this stimulus as compared to the stimulus trains. Moreover, the onset of the increase in $[Ca^{2+}]_N$ did not differ from that in $[Ca^{2+}]_S$ within the sampling interval of our recordings (33 ms). In contrast to our study, a significant delay (∼300 ms) was observed in carbachol-stimulated parotid acinar cells [33]. In these cells, the majority of mitochondria are localized around the nucleus and it was found that inhibitors of mitochondrial Ca^{2+} uptake abolished this delay suggesting the involvement of these organelles in propagation of the Ca^{2+} signal from the cytosol into the nucleus. The absence of such a delay in the present study then indicates that mitochondria localized in the perinuclear region in skeletal myotubes do not accumulate sufficient amounts of Ca^{2+} to interfere with Ca^{2+} signal propagation from the sarcoplasm to the nucleus. We therefore did not include perinuclear mitochondrial Ca^{2+} uptake in our mathematical model. Our mathematical model considers the decay in $[Ca^{2+}]_S$ as a first order process characterized by a single rate-constant (λ), accounting for all removal processes in the sarcoplasm (including SERCA-mediated Ca^{2+} uptake and mitochondrial Ca^{2+} uptake). Because mitochondrial Ca^{2+} uptake stimulates mitochondrial ATP production [34] and thus fuelling of the sarcoplasmic Ca^{2+} pumps [21], we can model the effect of reduced mitochondrial Ca^{2+} uptake on the sarcoplasmic and nuclear Ca^{2+} changes by increasing λ. The outcome can be tested using inhibitors of mitochondrial Ca^{2+} uptake.

Experimental data obtained with cardiac myocytes lead to the conclusion that Ca^{2+} diffused freely through NPCs at low cytosolic Ca^{2+} and that this diffusion was partially restricted at high cytosolic Ca^{2+} [40]. Our experiments show that the maximal amplitude of $[Ca^{2+}]_S$ remained the same when changing from a single stimulus to a train of stimuli. Therefore, our mathematical model required only a single value for the diffusion constant describing the diffusion across the nuclear envelope ($D_{SN} = 1\ \mu m^2/s$). This value was three-fold lower than that for the Ca^{2+} diffusion constant in the sarcoplasm ($D_S = 3\ \mu m^2/s$) and five-fold lower than that for the Ca^{2+} diffusion constant in the nucleus ($D_N = 5\ \mu m^2/s$). Increasing the value of D_{SN} from 0.5 to 2.8 $\mu m^2/s$ at a constant maximal amplitude of $[Ca^{2+}]_S$, increased both the rate of increase and the maximal amplitude of $[Ca^{2+}]_N$ (Fig. 3D). In contrast, this manoeuvre did not alter the time of onset of the $[Ca^{2+}]_N$ transient (Fig. 3D) nor improve the quantitative fit between model and experiment (Fig. 3A and B).

Previous work with hippocampal neurons revealed that electrical field stimulation led to a rapid translocation of calmodulin from the cytoplasm to the nucleus leading to a 2.4-fold increase within 42 s after the onset of stimulation [44]. However, quantitative modelling of the data obtained with skeletal myotubes required inclusion of a Ca^{2+} buffer (B) in the nuclei of unstimulated myotubes. This requirement mainly concerned the first single stimulus in that it allowed adjustment of the maximal amplitude of $[Ca^{2+}]_N$ and rate of nuclear $[Ca^{2+}]_N$ decay to experimental values. In contrast, inclusion of this buffer had virtually no effect on the kinetics of $[Ca^{2+}]_S$. During 1 Hz stimulation, however, the model predicts that the nuclear Ca^{2+} buffer is almost saturated. As a consequence, $[Ca^{2+}]_N$ increases to a value

that is markedly higher than observed for a single stimulus. From the fact that our model fully reproduces the sarcoplasmic and nuclear Ca^{2+} changes it can be concluded that the nuclear buffer capacity does not significantly change during the electrical stimulations. In other words, our model does not require a mobile Ca^{2+} buffer. Therefore, our model predicts that calmodulin molecules that enter the nucleus during electrical stimulation do not significantly add to the nuclear buffer capacity. In the presence of a nuclear Ca^{2+} buffer, changing D_{SN} had only minor effects. This indicates that the presence of the buffer, and not the semi-permeability of the nuclear membrane, is the dominant process in shaping $[Ca^{2+}]_N$. Evidence for the presence of nuclear Ca^{2+} buffers was obtained in pancreatic acinar cells [45], rat hepatocytes [46] and dopaminergic neurons [47]. Currently, we can only speculate about the molecular identity of the putative nuclear Ca^{2+} buffer in human skeletal myotubes because its predicted properties (K_d = 0.125 μM, $[B]_T$ = 1.5 μM) do not match with those of Indo-1 or one of the known nuclear Ca^{2+} binding proteins.

4.3. Physiological implications

Our experimental results indicate that although $[Ca^{2+}]_N$ is directly derived from $[Ca^{2+}]_S$, the frequency of the electrical stimulus determines whether AM of $[Ca^{2+}]_N$ occurs. It is tempting to speculate that such decoupling between sarcoplasmic and nuclear Ca^{2+} signals allows low-frequency $[Ca^{2+}]_S$ signals to stimulate contraction without transcription activation, whereas high-frequency $[Ca^{2+}]_S$ signals activate both contraction and transcription. This mechanism might underlie the observation that the temporal pattern of electrical input (i.e. motoneuron firing) determines whether a muscle fibre becomes slow oxidative or fast glycolytic [48].

One can hypothesize that the cell can adapt the Ca^{2+}-signalling mechanism to specific physiological requirements by varying the expression levels and/or kinetic properties of its constituents such as SERCA pumps, nuclear Ca^{2+} buffers and/or NPCs on a relatively fast (e.g. Ca^{2+}-mediated closure of NPCs) or slow timescale (e.g. SERCA isoform switching; [49]). This idea is supported by the observation in human skeletal muscle that SERCA activity and subtype expression depend on fibre type [50] and that transcription rates of SERCA and phospholamban genes change in response to chronic stimulation [51]. On the other hand, decoding of the Ca^{2+} signal might be altered by expression of CaMKII isoforms with different Ca^{2+}-dependent kinetics [52].

Although a nucleoplasmic reticulum has been demonstrated in a hepatic cell line [10], its existence in human skeletal muscle still awaits discovery. In this context, the present data and modelling results do not provide evidence for the presence of a nucleoplasmic reticulum in human skeletal myotubes. Our quantitative simulations predict that AM of $[Ca^{2+}]_N$ requires both semi-permeability of the nuclear membrane and nuclear Ca^{2+} buffering. However, the Ca^{2+} permeability of the nuclear membrane appears to be of minor importance in human skeletal myotubes.

References

[1] M.J. Berridge, P. Lipp, M.D. Bootman, The versatility and universality of calcium signalling, Nat. Rev. Mol. Cell Biol. 1 (2000) 11–21.

[2] M.J. Berridge, The endoplasmic reticulum: a multifunctional signaling organelle, Cell Calcium 32 (2002) 235–249.

[3] M.J. Berridge, M.D. Bootman, H.L. Roderick, Calcium signalling: dynamics, homeostasis and remodelling, Nat. Rev. Mol. Cell. Biol. 4 (2003) 517–529.

[4] G. Hajnoczky, L.D. Robb-Gaspers, M.B. Seitz, A.P. Thomas, Decoding of cytosolic calcium oscillations in the mitochondria, Cell 82 (1995) 415–424.

[5] G.E. Hardingham, S. Chawla, C.M. Johnson, H. Bading, Distinct functions of nuclear and cytoplasmic calcium in the control of gene expression, Nature 385 (1997) 260–265.

[6] Y. Kirichok, G. Krapivinsky, D.E. Clapham, The mitochondrial calcium uniporter is a highly selective ion channel, Nature 427 (2004) 360–364.

[7] N.L. Allbritton, E. Oancea, M.A. Kuhn, T. Meyer, Source of nuclear calcium signals, Proc. Natl. Acad. Sci. U.S.A. 91 (1994) 12458–12462.

[8] A.N. Malviya, P. Rogue, G. Vincendon, Stereospecific inositol 1,4,5-[^{32}P]trisphosphate binding to isolated rat liver nuclei: evidence for inositol trisphosphate receptor-mediated calcium release from the nucleus, Proc. Natl. Acad. Sci. U.S.A. 87 (1990) 9270–9274.

[9] M. Fricker, M. Hollinshead, N. White, D. Vaux, Interphase nuclei of many mammalian cell types contain deep, dynamic, tubular membrane-bound invaginations of the nuclear envelope, J. Cell Biol. 136 (1997) 531–544.

[10] W. Echevarria, M.F. Leite, M.T. Guerra, W.R. Zipfel, M.R. Nathanson, Regulation of calcium signals in the nucleus by a nucleoplasmic reticulum, Nat. Cell Biol. 5 (2003) 440–446.

[11] M.F. Leite, E.C. Thrower, W. Echevarria, P. Koulen, K. Hirata, A.M. Bennett, B.E. Ehrlich, M.H. Nathanson, Nuclear and cytosolic calcium are regulated independently, Proc. Natl. Acad. Sci. U.S.A. 100 (2003) 2975–2980.

[12] P.P. Lui, F.L. Chan, Y.K. Suen, T.T. Kwok, S.K. Kong, The nucleus of HeLa cells contains tubular structures for Ca^{2+} signaling with the involvement of mitochondria, Biochem. Biophys. Res. Comm. 308 (2003) 826–833.

[13] E. Jaimovich, R. Reyes, J.L. Liberona, J.A. Powell, IP_3 receptors, IP_3 transients, and nucleus-associated Ca^{2+} signals in cultured skeletal muscle, Am. J. Physiol. Cell Physiol. 278 (2000) C998–C1010.

[14] M. Estrada, C. Cardenas, J.L. Liberona, M.A. Carrasco, G.A. Mignery, P.D. Allen, E. Jaimovich, Calcium transients in 1B5 myotubes lacking ryanodine receptors are related to inositol trisphosphate receptors, J. Biol. Chem. 276 (2001) 22868–22874.

[15] J.A. Powell, M.A. Carrasco, D.S. Adams, B. Drouet, J. Rios, M. Müller, M. Estrada, E. Jaimovich, IP_3 receptor function and localization in myotubes: an unexplored Ca^{2+} signaling pathway in skeletal muscle, J. Cell Sci. 114 (2001) 3673–3683.

[16] J.D. Meissner, H.P. Kubis, R.J. Scheibe, G. Gros, Reversible Ca^{2+}-induced fast-to-slow transition in primary skeletal muscle culture cells at the mRNA level, J. Physiol. 523 (2000) 19–28.

[17] J.D. Meissner, G. Gros, R.J. Scheibe, M. Scholz, H.P. Kubis, Calcineurin regulates slow myosin, but not fast myosin or metabolic enzymes, during fast-to-slow transformation in rabbit skeletal muscle cell culture, J. Physiol. 533 (2001) 215–226.

[18] H.P. Kubis, N. Hanke, R.J. Scheibe, J.D. Meissner, G. Gros, Ca^{2+} transients activate calcineurin/NFATc1 and initiate fast-to-slow transformation in a primary skeletal muscle culture, Am. J. Physiol. Cell Physiol. 285 (2003) C56–C63.

[19] W.J.H. Koopman, M. Renders, A. Oosterhof, T.H. van Kuppevelt, B.G. Van Englen, A. Willems, Upregulation of Ca^{2+} removal in human skeletal muscle: a possible role for Ca^{2+}-dependent priming of mitochondrial ATP synthesis, Am. J. Physiol. Cell Physiol. 285 (2003) C1263–C1269.
[20] W.J.H. Koopman, W.J. Scheenen, R.J. Errington, P.H.G.M. Willems, R.J. Bindels, E.W. Roubos, B.G. Jenks, Membrane-initiated Ca^{2+} signals are reshaped during propagation to subcellular regions, Biophys. J. 81 (2001) 57–65.
[21] W.J.H. Koopman, R.R. Bosch, S.E. Van Emst-de Vries, M. Spaargaren, J.J.H.H.M. De Pont, P.H.G.M Willems, R-Ras alters Ca^{2+} homeostasis by increasing the Ca^{2+} leak across the endoplasmic reticular membrane, J. Biol. Chem. 278 (2003) 13672–13679.
[22] A.J.C. De Groof, J.A. Fransen, R.J. Errington, P.H.G.M. Willems, B. Wieringa, W.J.H. Koopman, The creatine kinase system is essential for optimal refill of the sarcoplasmic reticulum Ca^{2+} store in skeletal muscle, J. Biol. Chem. 277 (2002) 5275–5284.
[23] G.M. Jenniskens, W.J.H. Koopman, P.H.G.M. Willems, I. Pecker, J.H. Veerkamp, T.H. van Kuppevelt, Phenotypic knock out of heparan sulfates in myotubes impairs excitation-induced calcium spiking, FASEB J. 17 (2003) 878–880.
[24] A.A.G.M. Benders, A. Oosterhof, R.A. Wevers, J.H. Veerkamp, Excitation-contraction coupling of cultured human skeletal muscle cells and the relation between basal cytosolic Ca^{2+} and excitability, Cell Calcium 21 (1997) 81–91.
[25] F.H. Van de Put, J.J. De Pont, P.H. Willems, Heterogeneity between intracellular Ca^{2+} stores as the underlying principle of quantal Ca^{2+} release by inositol 1,4,5-trisphosphate in permeabilized pancreatic acinar cells, J. Biol. Chem. 269 (1994) 12438–12443.
[26] J.R. Lieste, W.J.H. Koopman, V.C. Reynen, W.J.J.M. Scheenen, B.G. Jenks, E.W. Roubos, Action currents generate stepwise intracellular Ca^{2+} patterns in a neuroendocrine cell, J. Biol. Chem. 273 (1998) 25686–25694.
[27] D.G. Allen, H. Westerblad, Role of phosphate and calcium stores in muscle fatigue, J. Physiol. 536 (2001) 657–665.
[28] A.M. Duke, D.S. Steele, Mechanism of reduced SR Ca^{2+} release induced by inorganic phosphate in rat skeletal muscle fibers, Am. J. Physiol. Cell Physiol. 281 (2001) C418–C429.
[29] B. Abrenica, J.S.C. Gilchrist, Nucleoplasmic Ca^{2+} loading is regulated by mobilization of perinuclear Ca^{2+}, Cell Calcium 28 (2000) 127–136.
[30] A. Nori, P. Lin, A. Cassetti, A. Villa, K.U. Bayer, P. Volpe, Targeting of α-kinase-anchoring protein (αKAP) to sarcoplasmic reticulum and nuclei of skeletal muscle, Biochem. J. 370 (2003) 873–880.
[31] J.L. Fox, A.D. Burgstahler, M.H. Nathanson, Mechanism of long-range Ca^{2+} signaling in the nucleus of isolated rat hepatocytes, Biochem. J. 326 (1997) 491–495.
[32] H. Tinel, J.M. Cancela, H. Mogami, J.V. Gerasimenko, O.V. Gerasimenko, A.V. Tepikin, O.H. Petersen, Active mitochondria surrounding the pancreatic acinar granule region prevent spreading of inositol trisphosphate-evoked local cytosolic Ca^{2+} signals, EMBO J. 18 (1999) 4999–5008.
[33] J.I. Bruce, D.R. Giovannucci, G. Blinder, T.J. Shuttleworth, D.I. Yule, Modulation of $[Ca^{2+}]_i$ signaling dynamics and metabolism by perinuclear mitochondria in mouse parotid acinar cells, J. Biol. Chem. 279 (2004) 12909–12917.
[34] H.J. Visch, G.A. Rutter, W.J.H. Koopman, J.B. Koenderink, S. Verkaart, T. de Groot, A. Varadi, K.J. Mitchell, L.P. Van den Heuvel, J.A.M. Smeitink, P.H.G.M. Willems, Inhibition of mitochondrial Na^+-Ca^{2+} exchange restores agonist-induced ATP production and Ca^{2+} handling in human complex I deficiency, J. Biol. Chem. 279 (2004) 40328–40336.
[35] M. Naraghi, T.H. Müller, E. Neher, Two-dimensional determination of the cellular Ca^{2+} binding in bovine chromaffin cells, Biophys. J. 75 (1998) 1635–1647.
[36] J.O. Bustamante, E.R. Michelette, J.P. Geibel, J.A. Hanover, T.J. McDonnell, D.A. Dean, Dendrimer-assisted patch-clamp sizing of nuclear pores, Pflugers Arch. 439 (2000) 829–837.
[37] P.J. Rogue, A.N. Malviya, Calcium signals in the cell nucleus, EMBO J. 18 (1999) 5147–5152.
[38] M.W. Berchtold, H. Brinkmeier, M. Müntener, Calcium ion in skeletal muscle: Its crucial role for muscle function, plasticity, and disease, Physiol. Rev. 80 (2000) 1215–1265.
[39] C. Perez-Terzic, L. Stehno-Bittel, D.E. Clapham, Nucleoplasmic and cytoplasmic differences in the fluorescence properties of the calcium indicator Fluo-3, Cell Calcium 21 (1997) 275–282.
[40] C. Genka, H. Ishida, K. Ichimori, Y. Hirota, T. Tanaami, H. Nakazawa, Visualization of biphasic Ca^{2+} diffusion from cytosol to nucleus in contracting adult rat cardiac myocytes with an ultra-fast confocal imaging system, Cell Calcium 25 (1999) 199–208.
[41] B.R. Wamhoff, D.K. Bowles, N.J. Dietz, Q. Hu, M. Sturek, Exercise training attenuates coronary smooth muscle phenotypic modulation and nuclear Ca^{2+} signaling, Am. J. Physiol. Heart Circ. Physiol. 283 (2002) H2397–H2410.
[42] M.D. Bootman, D. Thomas, S.C. Tovey, M.J. Berridge, P. Lipp, Nuclear calcium signaling, Cell. Mol. Life Sci. 57 (2000) 371–378.
[43] M.R. Duchen, Mitochondria in health and disease: perspectives on a new mitochondrial biology, Mol. Aspects Med. 25 (2004) 365–451.
[44] K. Deisseroth, E.K. Heist, R.W. Tsien, Translocation of calmodulin to the nucleus supports CREB phosphorylation in hippocampal neurons, Nature 392 (1998) 198–202.
[45] M. Craske, T. Takeo, O. Gerasimenko, C. Vaillant, K. Torok, O.H. Petersen, A.V. Tepikin, Hormone-induced secretory and nuclear translocation of calmodulin: oscillations of calmodulin concentration with the nucleus as an integrator, Proc. Natl. Acad. Sci. U.S.A. 96 (1999) 4426–4431.
[46] R. Bosser, R. Aligue, D. Guerini, N. Agell, E. Carafoli, O. Bachs, Calmodulin can modulate protein phosphorylation in rat liver cells nuclei, J. Biol. Chem. 268 (1993) 15477–15483.
[47] D.C. German, M.C. Ng, C.L. Liang, A. McMahon, A.M. Iacopino, Calbindin-D28k in nerve cell nuclei, Neuroscience 81 (1997) 735–743.
[48] E.N. Olson, R.S. Williams, Remodeling muscles with calcineurin, BioEssays 22 (2000) 510–519.
[49] C. Magnier, B. Papp, E. Corvazier, R. Bredoux, F. Wuytack, J. Eggermont, J. Maclouf, J. Enouf, Regulation of sarco-endoplasmic reticulum Ca^{2+}-ATPases during platelet-derived growth factor-induced smooth muscle cell proliferation, J. Biol. Chem. 267 (1992) 15808–15815.
[50] P. Szentesi, R. Zaremba, W. van Mechelen, G.J.M. Stienen, ATP utilization for calcium uptake and force production in different types of human skeletal muscle fibres, J. Physiol. 531 (2001) 393–403.
[51] P. Hu, K.M. Zhang, J.A. Spratt, A.S. Wechsler, F.N. Briggs, Transcription rates of SERCA and phospholamban genes changes in response to chronic stimulation of skeletal muscle, Biochim. Biophys. Acta 1395 (1998) 121–125.
[52] K.U. Bayer, P. de Koninck, H. Schulman, Alternative splicing modulates the frequency-dependent response of CaMKII to Ca^{2+} oscillations, EMBO J. 21 (2002) 3590–3597.